Received: 24 July 2019 | Revised: 2 September 2019 | Accepted: 5 September 2019

DOI: 10.1002/inf2.12044

ORIGINAL ARTICLE

WILEY

Solute manipulation enabled band and defect engineering for thermoelectric enhancements of SnTe

Zhichao Yao[1#] | Wen Li[1#] | Jing Tang[1] | Zhiwei Chen[1] | Siqi Lin[1] | Kanishka Biswas[2] | Alexander Burkov[3] | Yanzhong Pei[1]

[1]Interdisciplinary Materials Research Center, School of Materials Science and Engineering, Tongji University, Shanghai, China

[2]Jawaharlal Nehru Centre for Advanced Scientific Research (JNCASR), Bangalore, India

[3]Laboratory for Physics of Thermoelements, Ioffe Institute, Sankt-Petersburg, Russia

Correspondence
Yanzhong Pei, Interdisciplinary Materials Research Center, School of Materials Science and Engineering, Tongji University, 4800 Caoan Rd., Shanghai 201804, China.
Email: yanzhong@tongji.edu.cn

Funding information
"Shu Guang" Project Supported by Shanghai Municipal Education Commission and Shanghai Education Development Foundation, Shanghai Natural Science Foundation, Grant/Award Number: 19ZR1459900; Fok Ying Tung Education Foundation, Grant/Award Number: 20170072210001; Fundamental Research Funds for Science and Technology Innovation Plan of Shanghai, Grant/Award Number: 18JC1414600; Fundamental Research Funds for the Central Universities; National Key Research and Development Program of China, Grant/Award Number: 2018YFB-703600; National Natural Science Foundation of China, Grant/Award Numbers: 51772215, 51861145305; Russian Foundation for Basic Research, Grant/Award Number: 18-52-80005

Abstract

With years of development, SnTe as a homologue of PbTe has shown great potential for thermoelectric applications in *p*-type conduction, and the most successful strategy is typified by alloying for maximizing the valence band degeneracy. Among the known alloy agents, MnTe has been found to be one of the most effective enabling a band convergence for an enhancement in electronic performance of SnTe, yet its solubility of only ~15 at% unfortunately prevents a full optimization in the valence band structure. This work reveals that additional PbTe alloying not only promotes the MnTe solubility to locate the optimal valence band structure but also increases the overall substitutional defects in the material for a substantial reduction in lattice thermal conductivity. In addition, PbTe alloying simultaneously optimizes the carrier concentration due to the cation size effect. These features all enabled by such a solute manipulation synergistically lead to a very high thermoelectric figure of merit, zT of ~1.5 in SnTe with a 20 at% MnTe and a 30 at% PbTe alloying ($Sn_{0.5}Mn_{0.2}Pb_{0.3}Te$), demonstrating the effectiveness of solute manipulation for advancing SnTe and similar thermoelectrics.

KEYWORDS

band engineering, MnTe solubility, SnTe, thermoelectric

[#]Zhichao Yao and Wen Li contributed equally to this study.

1 | INTRODUCTION

Thermoelectrics enabling a direct conversion between heat and electricity based on either Seebeck or Peltier effect[1] have been widely considered as an sustainable energy technology. The conversion efficiency of thermoelectric materials is determined by the dimensionless figure of merit, $zT = S^2T/\rho(\kappa_E + \kappa_L)$, which depends on the Seebeck coefficient (S), the absolute temperature (T), the electrical resistivity (ρ), and the electronic (κ_E) and lattice (κ_L) thermal conductivity.[2] Thus, high-zT materials are critical for high-efficiency and large-scale thermoelectric applications, which motivates numerous efforts to be put on zT enhancements of thermoelectric materials.

Owing to the strong coupling effects among S, ρ, and κ_E via carrier concentration, band structure, and scattering of carriers, historical efforts for zT enhancements have been devoted to minimizing κ_L, the only independent parameter determining zT. This can be realized by the introduction of various defects, such as point defects,[3,4] dislocations,[5-8] and nanostructures,[9-11] for strengthening phonon scattering due to the introduced mass and strain fluctuations.[12,13] Alternatively, complex crystal structures,[14] soft chemical bonds,[15-17] low sound velocity,[15] low acoustic cut-off frequency,[18] strong lattice anharmonicity,[19,20] and liquid-like ions[21-23] are found to be effective sources leading to a low κ_L.

Band engineering[24-26] approaches, typified by band convergence,[25,27] are demonstrated to be successful as well, in terms of decoupling the relationship among the strongly coupled electronic properties at some degree for electronic enhancements. This has led to significant zT improvements in various materials such as PbTe,[28-31] half-Heusler,[32-35] SnTe,[36-38] silicides,[39-41] GeTe,[42-45] Zintl phase,[46,47] and Te.[48] However, it should be noted that an optimal carrier concentration (n) is always required to realize the maximal performance for a given material because electronic transport properties are optimized in a certain narrow range of reduced Fermi level.[2]

Utilization of these proven strategies has frequently realized significantly enhanced zT in p-type PbTe thermoelectrics. This largely stems from the coexistence of L and Σ valence bands, of which, respectively, have a high band degeneracy (N_v) of 4 and 12. Importantly, the energy offset between ($\Delta E_{L\text{-}\Sigma}$) can be engineered to be within a few k_BT[49,50] for an overall high N_v of 12 to 16 thus leading to an enhanced power factor ($PF = S^2/\rho$). With a further help of microstructure engineering for κ_L reduction, an extraordinary zT (>2) has been achieved.[7,44]

As a homolog to PbTe with the same crystal structure and similar band structure, SnTe has been considered as a potentially promising thermoelectric material as well. Unfortunately, compared with PbTe, SnTe shows a much larger $\Delta E_{L\text{-}\Sigma}$ of 12 to 15 k_BT at room temperature,[51] and the lighter atomic mass leads to a much higher lattice thermal conductivity.[37,52] Eventually, pristine SnTe even with an optimal carrier concentration shows a peak zT of only 0.6 at 700 K.[53]

Greatly inspired by the successful strategies for zT enhancements realized in PbTe with alloying, monotelluride solutes such as MnTe,[37,54,55] MgTe,[56-58] CdTe,[59-61] CaTe,[62] and HgTe[63] are found to successfully minimize the $\Delta E_{L\text{-}\Sigma}$ for an electronic improvement of SnTe. Among these solutes, MnTe is found to be one of the most effective for maximizing the valence band degeneracy (N_v) due to its high solubility of ~15 at%.[37] Fortunately, the solubility of MnTe in SnTe is found to be further increased up to 25 at% with an additional 5 at% GeTe alloying ($Sn_{0.7}Ge_{0.05}Mn_{0.25}Te$).[54] Such an increase in MnTe solubility enables a further N_v maximization through an involvement of new highly degenerated transporting band (Λ).[54] A similar effect on increasing N_v due to the increase of solubility is also found in SnTe with a MgTe alloying.[64]

It should be noted that a high zT realized in above mentioned alloys usually involves a further Cu_2Te alloying[54,64,65] for a sufficiently reduced κ_L through the strong phonon scattering by Cu interstitials[52] and an excess of Sn for reducing the carrier concentration. Precipitation of excessive Sn and Cu_2Te particularly at low temperatures[54,56,64,65] might lead to diffusion problems for practical applications. This motivates the search of single-phase solid solutions with a comparable or even higher zT.

One noticeable challenging is that the increase of MnTe alloying leads to a significant deviation in carrier concentration from its optimum.[37] An effective approach is inspired by the feature that the carrier concentration of IV-VI tellurides is closely related to the size of cation.[66-68] In more details, a gradual increase in cation size from Ge to Sn and then to Pb leads to a decrease in intrinsic carrier concentration from GeTe to SnTe and then to PbTe by orders of magnitude.[69-71] This indicates that an increase in the mean size of cations such as by PbTe alloying might lead to an effective reduction in carrier concentration, an effect of which has been observed in GeTe with Pb/Ge substitutions[68] and SnTe-PbTe.[66,67] This effect is also related to a decrease upon such substitution of the equilibrium vacancy concentration in the metal sublattice, which in SnTe act as acceptors.[72-74] In addition, PbTe alloying has shown the capability for increasing the solubility of MnTe in SnTe.[75] Furthermore, the high overall concentration of alloy defects introduced is expected to strengthen the phonon scattering for reducing κ_L.

Motivated by the above reasons, this work focuses on the thermoelectric properties of PbTe and MnTe alloyed SnTe,

with an attempt of simultaneously achieving a high valence band degeneracy,[7] a high overall concentration of substitutional defects, and an optimized carrier concentration in single-phase solid solutions. It is found that PbTe alloying enables not only an increase in MnTe solubility for an inclusion of maximal transporting valence bands and an increase in mean cation size for a reduction in carrier concentration but also a strengthening in phonon scattering for a minimization in lattice thermal conductivity. All these synergic effects successfully enable a revelation of a peak zT as high as ~1.5 in single-phase solid solution of $Sn_{0.5}Mn_{0.2}Pb_{0.3}Te$.

2 | MATERIALS AND METHODS

Polycrystalline $Sn_{1-x-y}Pb_xMn_yTe$ ($0.1 \le x \le 0.4$, $0.1 \le y \le 0.3$) was synthesized by melting the stoichiometric amounts of high-purity elements Sn (99.99%), Te (99.99%), Pb (99.999%), and Mn (99.98%) at 1223 K for 6 hours, quenching in cold water and annealing at 950 K for 48 hours. In order to characterize the microstructure, scanning electronic microscopy (SEM) equipped with an energy dispersive spectrometer (EDS) was used. The obtained ingots were hand ground into fine powder for X-ray diffraction (XRD) and hot pressing. Dense samples (>97% of the theoretical density) with ~12 mm in diameter and ~1.5 mm in thickness were obtained by an induction heating hot press system[76] at 900 K for 20 minutes under a uniaxial pressure of ~70 MPa.

The electrical transport properties including resistivity, Seebeck coefficient, and Hall coefficient were simultaneously measured on the pellet samples. The resistivity and Hall coefficient (R_H) were measured using the van der Pauw technique under a reversible magnetic field of 1.5 T. The Seebeck coefficient was obtained from the slope of the thermopower vs temperature gradients within 0 to 5 K.[77] Thermal diffusivity (D) was measured using a laser flash technique with the Netzsch LFA457 system, the heat capacity was determined by $C_p(k_B/\text{atom}) = [3.07 + 0.00047(T/\text{K}-300)]$,[78,79] where T is the absolute temperature. This simple equation is obtained by fitting the reported experimental data of Blachnik, within an uncertainty of 5% for all the lead chalcogenides and tin telluride.[80] The thermal conductivity was calculated via $\kappa = dC_pD$, where d is the density measured using the mass and geometric volume of the pellet. The measurement temperatures are in the range of 300 to 900 K for resistivity, Seebeck coefficient, and thermal diffusivity and 300 to 850 K for Hall coefficient. The measurement uncertainty for each transport property is about 5%. Both longitudinal and transverse sound velocities were measured using an ultrasonic pulse receiver (Olympus-NDT) equipped with an oscilloscope (Keysight). The optical absorption was measured using diffuse reflectance spectroscopy (Bruker Tensor II equipped with a diffuse reflectance attachment) at room temperature.

3 | RESULTS AND DISCUSSION

Room temperature XRD patterns for the samples are shown in Figure 1A and Figure S1. All the diffraction peaks in $Sn_{0.8-x}Mn_{0.2}Pb_xTe$ ($0.12 \le x \le 0.3$; Figure 1A) can be well indexed to the rock-salt structure, indicating the formation of

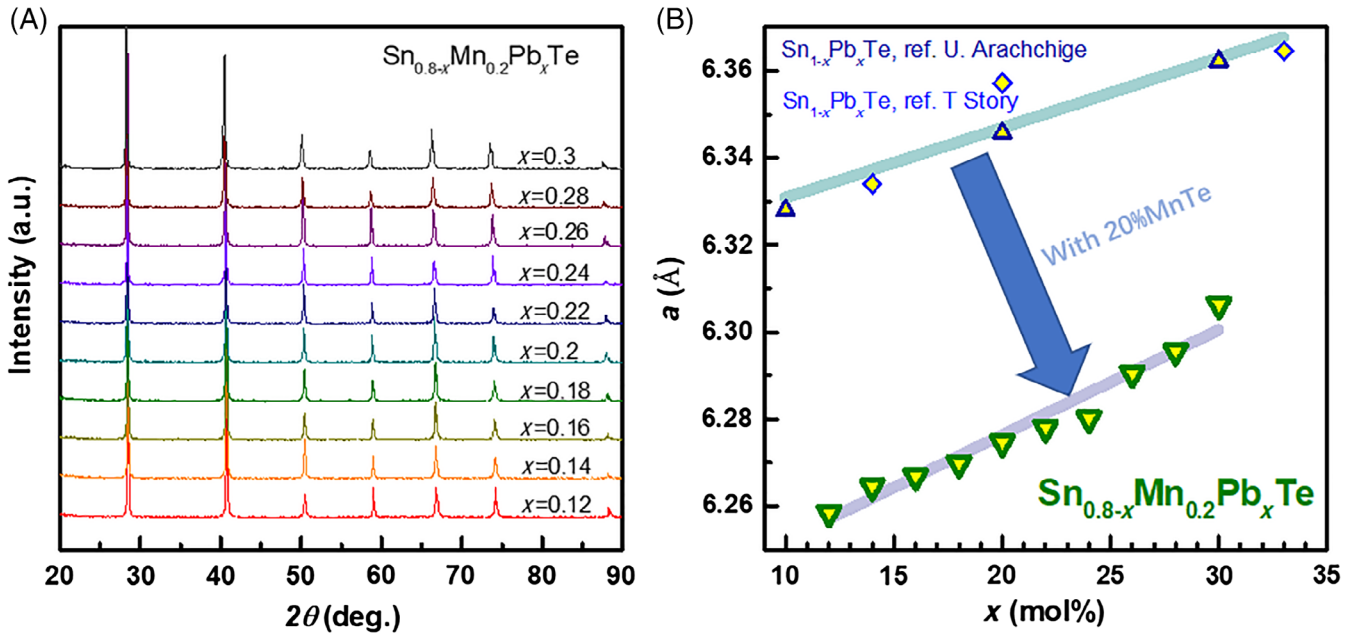

FIGURE 1 Room temperature X-ray diffraction patterns (A) and composition-dependent lattice parameters (B) for $Sn_{0.8-x}Mn0.2Pb_xTe$ ($0.12 \le x \le 0.3$)

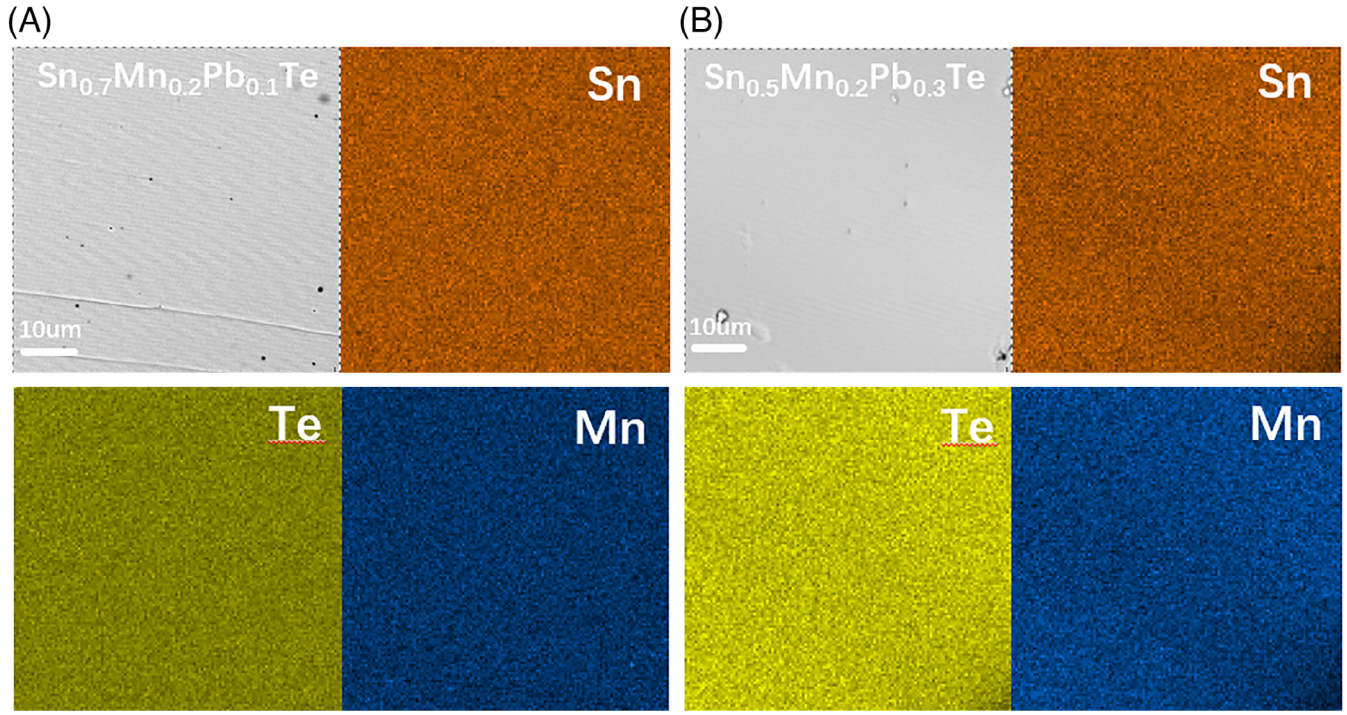

FIGURE 2 Scanning electronic microscope images and energy dispersive spectrometer mappings for $Sn_{0.8}Mn_{0.2}Pb_{0.1}Te$ (A) and $Sn_{0.5}Mn_{0.2}Pb_{0.3}Te$ (B)

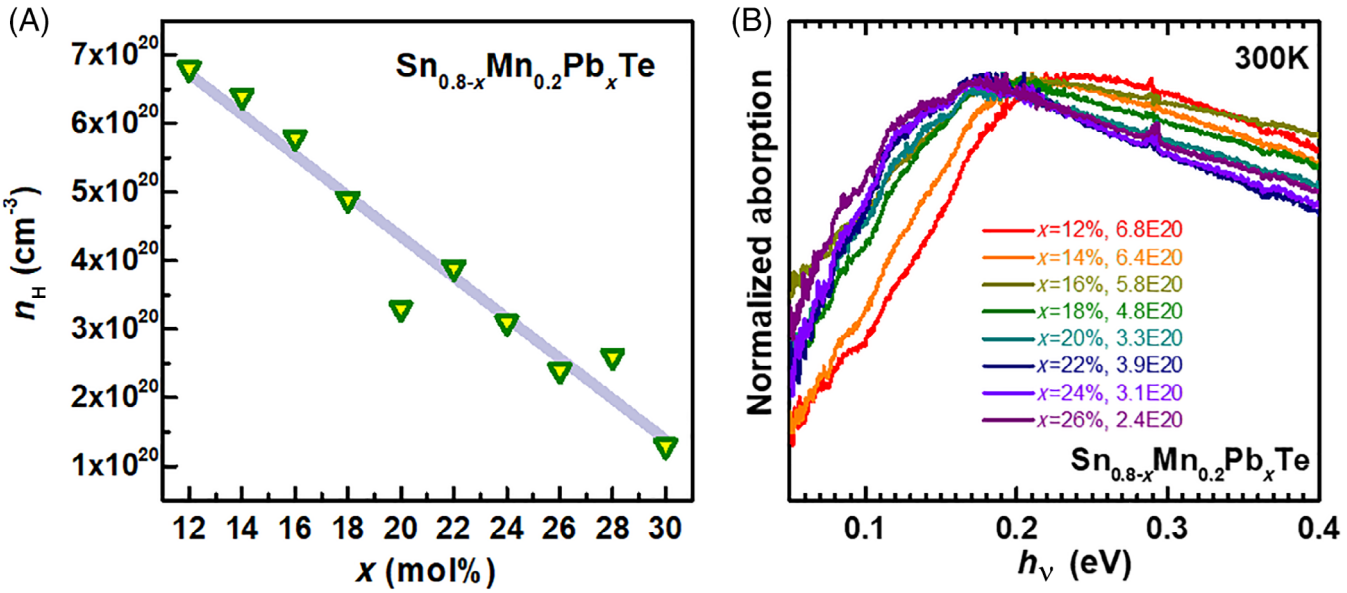

FIGURE 3 Composition-dependent Hall carrier concentration (n_H) (A) and photon energy–dependent absorption by free carriers (B) for $Sn_{0.8-x}Mn_{0.2}Pb_xTe$ at room temperature

single-phase solid solutions. This suggests a successful increase in MnTe solubility to 20 at% enabled by a 10 to 30 at% PbTe alloying. Once the MnTe concentration is higher than 25 at%, no solid solution region is found within a PbTe concentration of 10 to 40 at%. The formation of solid solutions in $Sn_{0.8-x}Mn_{0.2}Pb_xTe$ ($0.12 \leq x \leq 0.3$) is confirmed by SEM observations and EDS mapping analyses as shown in Figure 2A,B. Composition within the miscibility gap leads to the formation of MnTe impurities as verified by the SEM observations (Figure S2). This work focuses on solid

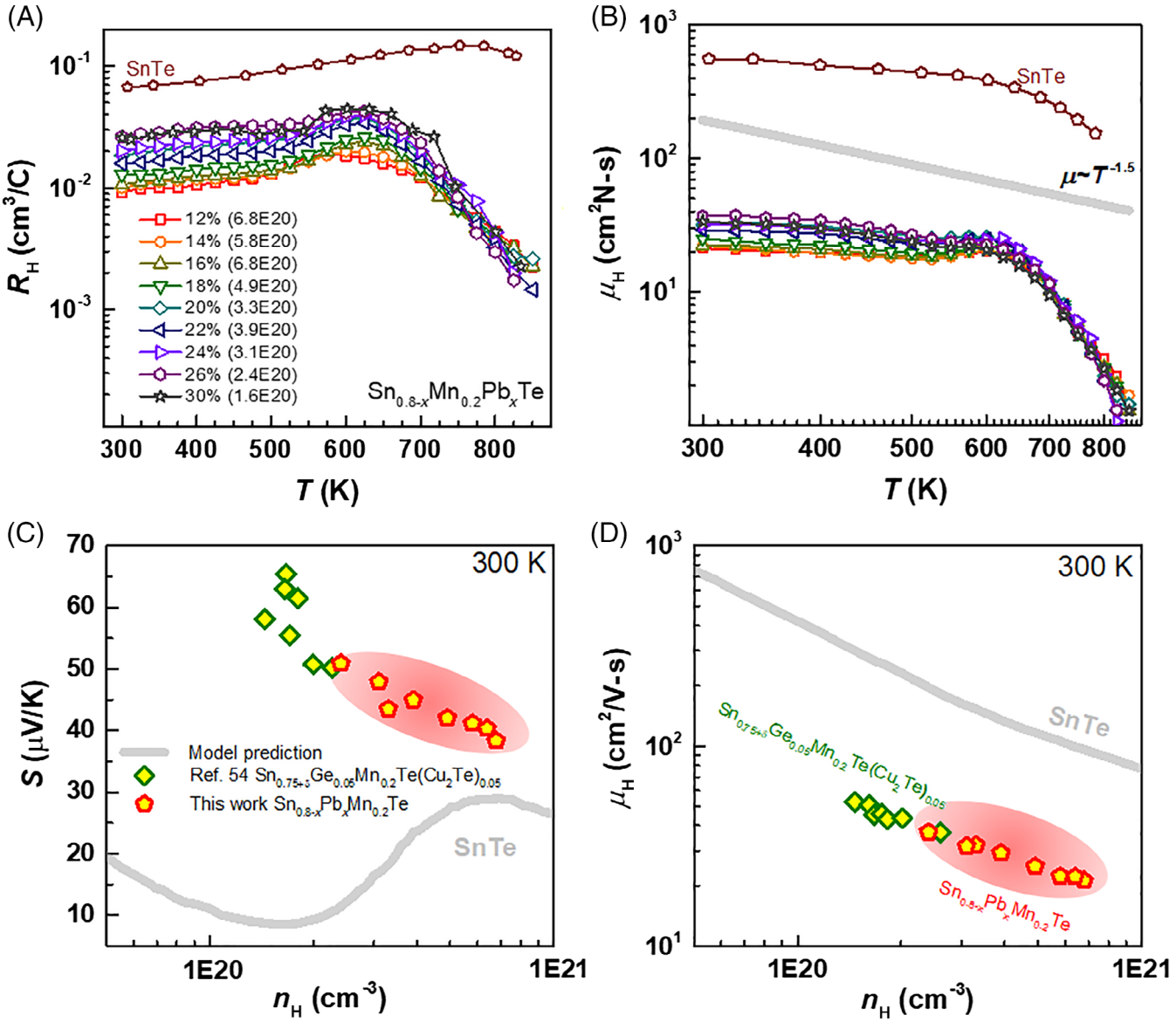

FIGURE 4 Temperature-dependent Hall coefficient (R_H) (A) and Hall mobility (m_H) (B) and room-temperature Hall carrier concentration–dependent Seebeck coefficient (C) and Hall mobility (D) for $Sn_{0.8-x}Mn_{0.2}Pb_xTe$, with a comparison to literature modeling and measurements[37,54]

solutions of $Sn_{0.8-x}Mn_{0.2}Pb_xTe$ ($0.1 \le x \le 0.3$), of which a MnTe concentration of 20 at% is found to maximize the valence band degeneracy according to the literature work.[54] The lattice parameter for $Sn_{0.8-x}Mn_{0.2}Pb_xTe$ is found to increase linearly with increasing x (Figure 1B), which can be well understood by the larger atomic size of Pb than that of Sn.

The origin of the increase in the solubility of MnTe in SnTe by addition of PbTe is not entirely sure. However, this might be closely related to the cation size effect, as with a decrease in cation size from Pb to Sn and then to Ge the crystal structure transits from a cubic structure for PbTe and SnTe to a rhombohedral structure for GeTe at room temperature. Because MnTe alloying decreases the lattice parameter of SnTe, a further PbTe alloying would compensate such a lattice shrinkage for stabilizing the cubic structure, which might promote the solubility of MnTe. However, in SnTe heavily alloyed with PbTe, the formation of MnTe precipitates could be understood by the limited solubility of MnTe in PbTe. Nevertheless, the observed change in MnTe solubility in this work is very similar to that in the literature.[75]

As the increase in mean size of cations accompanies with a reduction of carrier concentration in IV-VI thermoelectrics,[66-68] a reduction of carrier concentration is expected in $Sn_{0.8-x}Mn_{0.2}Pb_xTe$ with increasing x. Indeed, it is found that the Hall carrier concentration (n_H) linearly decreases from ~7×10^{20} to ~2×10^{20}/cm^3 with increasing x (Figure 3A), which can be roughly understood by the increased mean size of cations by PbTe alloying because of a decrease upon Pb/Sn substitution of the equilibrium cation

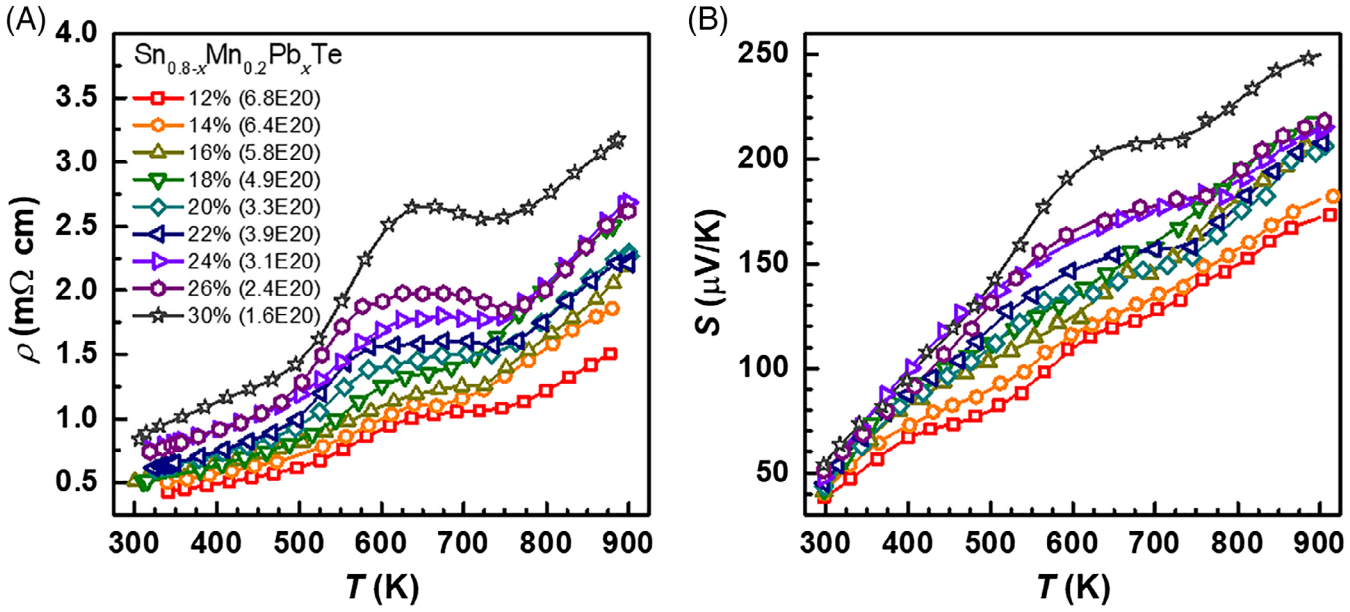

FIGURE 5 Temperature-dependent Seebeck coefficient (A) and resistivity (B) for $Sn_{0.8-x}Mn_{0.2}Pb_xTe$

vacancy concentration.[72-74] Similar cation-sized effect on carrier concentration has been found in GeTe thermoelectrics.[68]

Optical measurements at room temperature for $Sn_{0.8-x}Mn_{0.2}Pb_xTe$ are shown in Figure 3B. The observed shift of the absorption maximum to lower energies indicates a lowering of Fermi level in agreement with decreasing n_H. Furthermore, the optical measurements enable an estimation of inertial effective mass (m_I*) using the Lyden method[81] via the equation of $w_p^2 = ne^2/m_I^*\varepsilon_\infty\varepsilon_0$, where the w_p is the angular frequency of the absorption maximum (Figure 3B), n is the carrier concentration, e is the electronic charge, $\varepsilon_\infty = 48$ is the relative dielectric constant at the high frequency limit,[82,83] and ε_0 is the permittivity of free space. The estimated m_I* shows no obvious change due to PbTe alloying (Table S1).

Temperature-dependent Hall coefficient (R_H) and Hall mobility (μ_H) are shown in Figure 4A,B, respectively. Temperature peaking Hall coefficient, stemming from the redistribution of the carriers between different valence bands with different mobilities, has been commonly considered as an indication of band convergence in SnTe.[36] Comparing to pristine SnTe, a distinct reduction in the peak temperature for $Sn_{0.8-x}Mn_{0.2}Pb_xTe$ alloys indicates the convergence of valence bands. Due to the increased carrier concentration and carrier scattering by Mn/Sn substitutional defects, the samples show a lower μ_H as compared with that of pristine SnTe. Moreover, the increase in μ_H with increasing PbTe concentration mainly results from the reduced n_H. Importantly, temperature-dependent μ_H for $Sn_{0.8-x}Mn_{0.2}Pb_xTe$ shows a similar tendency with that of pristine SnTe, indicating an unchanged charge carrier scattering by acoustic phonons.

Room-temperature Hall carrier concentration–dependent Seebeck coefficient and Hall mobility for $Sn_{0.8-x}Mn_{0.2}Pb_xTe$ are shown in Figure 4C,D, respectively. It is found that Seebeck coefficient for the samples obtained in this work is much higher than the model prediction (gray curve in Figure 4C) for pristine SnTe, which further confirms the convergence of valence bands leading to an increased density of state effective mass. Due to the additional carrier scattering coming from the Pb/Sn and Mn/Sn substitutions, μ_H for all the samples is lower than that of pristine SnTe (gray curve in Figure 4D). The tendency of the increase in S and μ_H with decreasing n_H is quite similar with that of $Sn_{0.75+x}Ge_{0.05}Mn_{0.2}Te(Cu_2Te)_{0.05}$.[65] Therefore, SnTe alloys obtained in this work enable a very comparable electronic performance to that of $Sn_{0.75+\delta}Ge_{0.05}Mn_{0.2}Te(Cu_2Te)_{0.05}$ with the highest zT among SnTe thermoelectrics so far.[65]

Figure 5A,B shows temperature-dependent resistivity (ρ) and Seebeck coefficient (S) for $Sn_{0.8-x}Mn_{0.2}Pb_xTe$, respectively. The increase in both S and ρ with increasing temperature suggests a degenerated semiconducting behavior in all samples. Both resistivity and Seebeck coefficient increase in the entire temperature range with increasing PbTe concentration, which dominantly results from the decreased n_H. In addition, it is known that alloying SnTe with PbTe decreases the band gap (band gap equals to zero in $Sn_{0.4}Pb_{0.6}Te$ as a topological crystalline insulator[84,85]), whereas this is compromised by the 20 at% MnTe alloying as Mn/Pb substitution tends to increase the band gap.[86] Nevertheless, no strong indication of bipolar conduction is observed in this work.

Temperature-dependent total (κ) and lattice (κ_L) thermal conductivity for $Sn_{0.8-x}Mn_{0.2}Pb_xTe$ are shown in

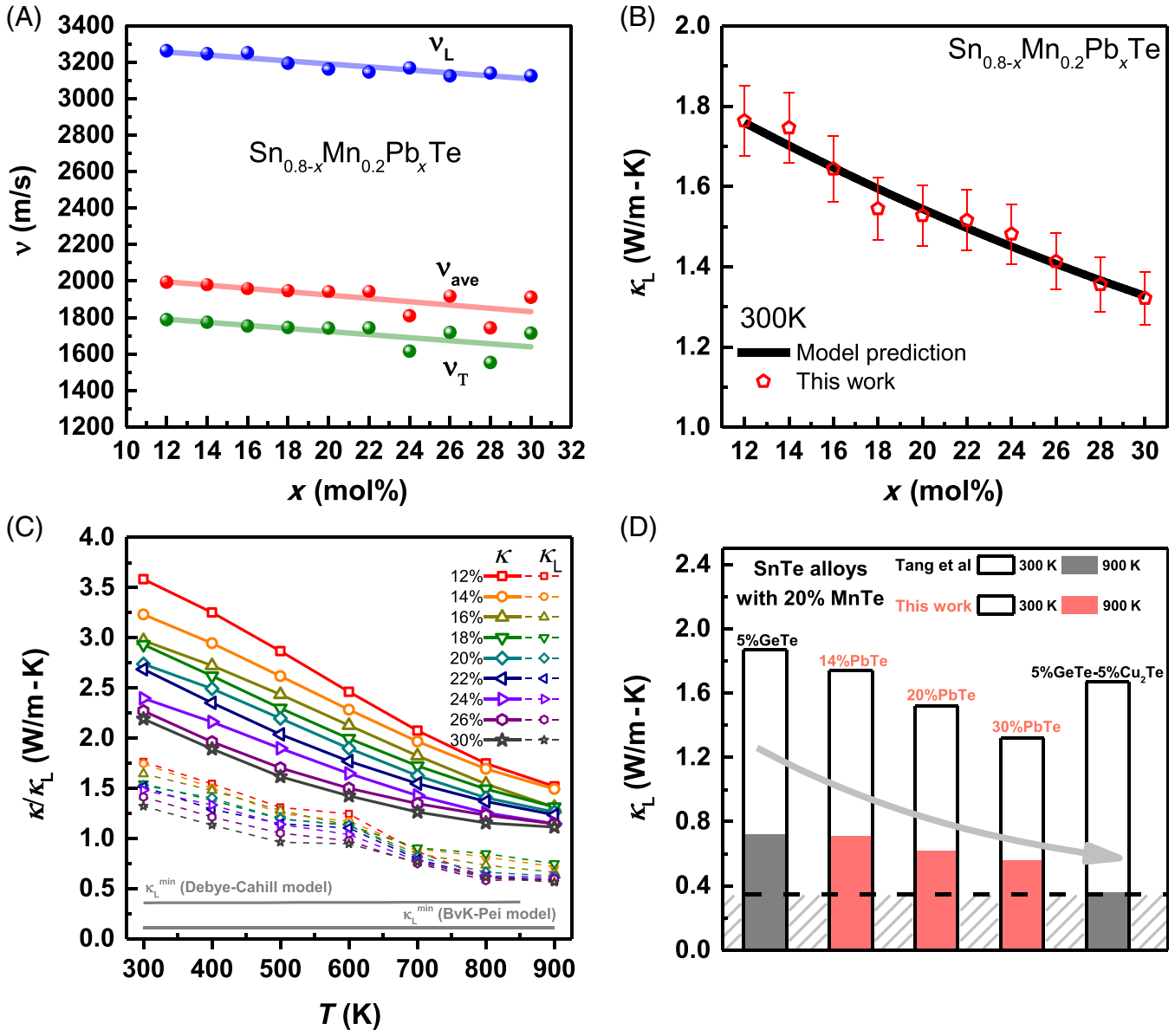

FIGURE 6 Composition-dependent sound velocities (A) and lattice thermal conductivity (κ_L) with a model prediction (black curve) for $Sn_{0.8-x}Mn_{0.2}Pb_xTe$ at 300 K (B). Temperature-dependent total (κ) and lattice (κ_L) thermal conductivity (C) and a comparison of κ_L with literature results for materials containing 20% MnTe alloying[37,54] at 300 and 900 K (D). The amorphous limit of κ_L is also included for comparison, which is estimated by either Debye-Cahill model[87] or a recently developed model taking into account the Born von Karman boundary conditions[88,89]

Figure 6C. The lattice thermal conductivity is estimated by subtracting the electronic contribution according to Wiedemann-Franz law ($\kappa_e = LT/\rho$) from total thermal conductivity, where L is the Lorenz factor determined by a single parabolic band model with acoustic phonon scattering.[87] Both κ and κ_L decrease with increasing temperature and PbTe concentration. The reduction in κ_L largely stems from the additional phonon scattering by Mn/Sn and Pb/Sn point defects introduced. As a result, the lowest κ_L of 0.5 W/m K is achieved in this work. This approaches the amorphous limit of SnTe estimated by the Debye-Cahill model (gray line in Figure 6C),[88] but there is still available room for a further reduction according to a recently developed model taking into account the periodic boundary conditions.[89,90] It is worth noticing that the lowest κ_L in this work is comparable to that of literature high-zT $Sn_{0.75+\delta}Ge_{0.05}Mn_{0.2}Te(Cu_2Te)_{0.05}$ alloys.[54] In addition to the cubic structure of SnTe alloys involved in this work, the thermoelectric properties are therefore believed to be isotropic.

In order to quantitatively evaluate the contribution of both Mn/Sn and Pb/Sn substitutional defects to the κ_L reduction, sound velocities for all the samples are measured at

TABLE 1 Mass density and estimated physical parameters according to sound velocity measurements for $Sn_{0.8-x}Mn_{0.2}Pb_xTe$ at room temperature

Pb content	θ_D (K)	ε	G (Gpa)	B (Gpa)	γ	d (g/cm^3)
$X = 12\%$	191	0.28	21.7	42.6	1.6	6.79
$X = 14\%$	189	0.28	21.5	43.6	1.7	6.85
$X = 16\%$	187	0.28	21.2	42.2	1.6	6.92
$X = 18\%$	186	0.28	21.1	41.3	1.6	6.96
$X = 20\%$	186	0.28	21.2	41.0	1.6	7.00
$X = 22\%$	188	0.33	21.5	57.1	1.9	7.09
$X = 24\%$	173	0.32	18.3	46.1	1.9	7.03
$X = 26\%$	183	0.28	21.0	41.6	1.6	7.14
$X = 28\%$	167	0.33	17.3	47.8	2.0	7.20
$X = 30\%$	183	0.28	21.4	42.6	1.6	7.29

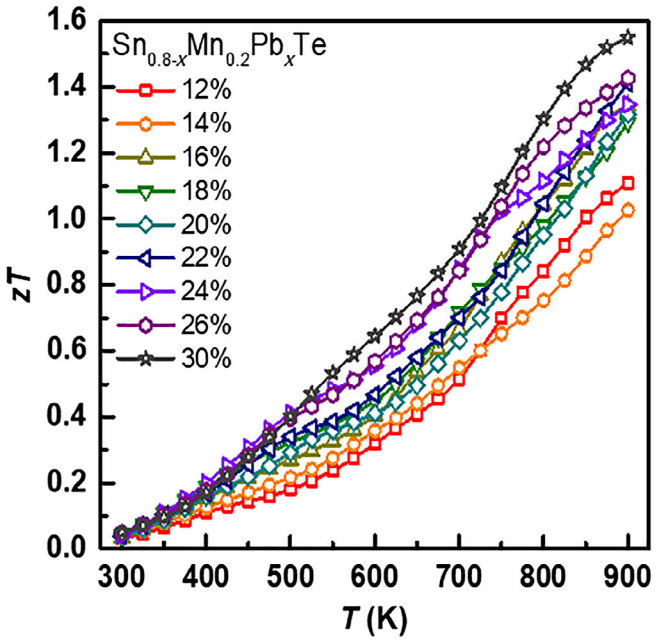

FIGURE 7 Temperature-dependent figure of merit (zT) for $Sn_{0.8-x}Mn_{0.2}Pb_xTe$

room temperature and shown in Figure 6A. It is seen that both transverse (ν_T) and longitudinal (ν_L) sound velocities decrease linearly with increasing PbTe content, which could be understood by the heavier atomic mass of substitutional Pb as compared with that of Sn. The measured sound velocities enable an estimation of physical parameters including Debye temperature (θ_D), Poisson ratio (ε), shear (G) and bulk (B) modulus, and Grüneisen parameter (γ).[91,92] The corresponding results are listed in Table 1. Using the measured sound velocities, composition-dependent κ_L for $Sn_{0.8-x}Mn_{0.2}Pb_xTe$ at room temperature can be reasonable predicted by recently developed model taking into account the periodic boundary conditions.[89] The detailed model prediction can be found in Supporting Information.

With the synergistic effects of band convergence by increased MnTe alloying concentration for electronic performance enhancement, an optimization of carrier concentration by the cation size manipulation, and strong phonon scattering by point defects for κ_L reduction, thermoelectric figure of merit (zT) is successfully improved to 1.5 for $Sn_{0.8-x}Mn_{0.2}Pb_xTe$ (Figure 7), which is comparable to the highest zT reported so far for SnTe thermoelectrics.[65] In addition, the high performance is found to be highly reproducible and thermally stable (Figure S3).

4 | SUMMARY

In summary, alloying SnTe with PbTe enables an increase in solubility of MnTe that leads to optimally converged valence bands for enhancing the electronic performance of SnTe. The involvement of PbTe alloying optimizes the carrier concentration due to cation size effect. Moreover, the high overall concentration of Mn/Sn and Pb/Sn substitutions enables strong a phonon scattering for minimizing the lattice thermal conductivity to 0.5 W/m K. These synergistic effects, all enabled by a solute manipulation, successfully lead to a realization of a peak zT as high as ~1.5 in single-phase solid solution $Sn_{0.5}Mn_{0.2}Pb_{0.3}Te$, being one of the highest realized in SnTe thermoelectrics.

ACKNOWLEDGEMENTS

This work is supported by the National Key Research and Development Program of China (2018YFB0703600), the National Natural Science Foundation of China (51861145305 [the BRICS project] and 51772215), Fundamental Research Funds for Science and Technology

Innovation Plan of Shanghai (18JC1414600), the Fok Ying Tung Education Foundation (20170072210001), "Shu Guang" Project Supported by Shanghai Municipal Education Commission and Shanghai Education Development Foundation, Shanghai Natural Science Foundation (19ZR1459900) and the Fundamental Research Funds for the Central Universities. A.B. acknowledges support by Russian Foundation for Basic Research under grant 18-52-80005 (BRICS).

ORCID

Yanzhong Pei https://orcid.org/0000-0003-1612-3294

REFERENCES

1. Bell LE. Cooling, heating, generating power, and recovering waste heat with thermoelectric systems. *Science*. 2008;321(5895):1457-1461.
2. Ioffe AF. *Semiconductor Thermoelements, and Thermoelectric Cooling*. London: Infosearch; 1957.
3. Zhang J, Xu B, Wang L-M, et al. Great thermoelectric power factor enhancement of CoSb3 through the lightest metal element filling. *Appl Phys Lett*. 2011;98(7):072109.
4. Shi X, Yang J, Salvador JR, et al. Multiple-filled Skutterudites: high thermoelectric figure of merit through separately optimizing electrical and thermal transports. *J Am Chem Soc*. 2011;133(20):7837-7846.
5. Chen ZW, Ge BH, Li W, et al. Vacancy-induced dislocations within grains for high-performance PbSe thermoelectrics. *Nat Commun*. 2017;8:13828.
6. Kim SI, Lee KH, Mun HA, et al. Thermoelectrics dense dislocation arrays embedded in grain boundaries for high-performance bulk thermoelectrics. *Science*. 2015;348(6230):109-114.
7. Wu Y, Chen Z, Nan P, et al. Lattice strain advances thermoelectrics. *Joule*. 2019;3:1276-1288.
8. Urban JJ. Anharmonic convergence: tuning two dials on phonons for high zT in p-type PbTe. *Joule*. 2019;3(5):1180-1181.
9. Shuai J, Geng H, Lan Y, et al. Higher thermoelectric performance of Zintl phases (Eu0.5Yb0.5)1-xCaxMg2Bi2 by band engineering and strain fluctuation. *Proc Natl Acad Sci U S A*. 2016;113(29):E4125-E4132.
10. Poudel B, Hao Q, Ma Y, et al. High-thermoelectric performance of nanostructured bismuth antimony telluride bulk alloys. *Science*. 2008;320(5876):634-638.
11. Xie W, He J, Kang H, Tang X, Zhu S, Laver M. Identifying the specific nanostructures responsible for the high thermoelectric performance of (Bi,Sb)(2)Te-3 nanocomposites. *Nano Lett*. 2010;10(9):3283-3289.
12. Klemens PG. The scattering of low-frequency lattice waves by static imperfections. *Proc Phys Soc*. 1955;A68(12):1113-1128.
13. Carruthers P. Scattering of phonons by elastic strain fields and the thermal resistance of dislocations. *Phys Rev*. 1959;114(4):995-1001.
14. Snyder GJ, Toberer ES. Complex thermoelectric materials. *Nat Mater*. 2008;7(2):105-114.
15. Li W, Lin SQ, Ge BH, Yang J, Zhang WQ, Pei YZ. Low sound velocity contributing to the high thermoelectric performance of Ag_8SnSe_6. *Adv Sci (Weinh)*. 2016;3(11):1600196.
16. Ying P, Li X, Wang Y, et al. Hierarchical chemical bonds contributing to the intrinsically low thermal conductivity in α-MgAgSb thermoelectric materials. *Adv Funct Mater*. 2017;27(1):1604145.
17. Li W, Lin S, Weiss M, et al. Crystal structure induced ultralow lattice thermal conductivity in thermoelectric Ag9AlSe6. *Adv Energy Mater*. 2018;8(18):1800030.
18. Lin S, Li W, Li S, et al. High thermoelectric performance of Ag_9GaSe_6 enabled by low cutoff frequency of acoustic phonons. *Joule*. 2017;1:816-830.
19. Li CW, Hong J, May AF, et al. Orbitally driven giant phonon anharmonicity in SnSe. *Nat Phys*. 2015;11(12):1063-1069.
20. Chang C, Zhao L-D. Anharmoncity and low thermal conductivity in thermoelectrics. *Mater Today Phys*. 2018;4:50-57.
21. Liu H, Shi X, Xu F, et al. Copper ion liquid-like thermoelectrics. *Nat Mater*. 2012;11(5):422-425.
22. Liu H, Yuan X, Lu P, et al. Ultrahigh thermoelectric performance by electron and phonon critical scattering in Cu2Se1-xIx. *Adv Mater*. 2013;25(45):6607-6612.
23. Zhao K, Qiu P, Song Q, et al. Ultrahigh thermoelectric performance in Cu 2−y Se 0.5 S 0.5 liquid-like materials. *Mater Today Phys*. 2017;1:14-23.
24. Pei YZ, Wang H, Snyder GJ. Band engineering of thermoelectric materials. *Adv Mater*. 2012;24(46):6125-6135.
25. Pei YZ, Shi X, LaLonde A, Wang H, Chen LD, Snyder GJ. Convergence of electronic bands for high performance bulk thermoelectrics. *Nature*. 2011;473(05 May):66-69.
26. Zaitsev VK, Fedorov MI, Gurieva EA, et al. Highly effective Mg2Si1−xSnx thermoelectrics. *Phys Rev B*. 2006;74(4):045207.
27. Yang L, Chen Z-G, Dargusch MS, Zou J. High performance thermoelectric materials: progress and their applications. *Adv Energy Mater*. 2018;8(6):1701797.
28. Chen ZW, Jian ZZ, Li W, et al. Lattice dislocations enhancing thermoelectric PbTe in addition to band convergence. *Adv Mater*. 2017;29(23):1606768.
29. Pei YZ, LaLonde AD, Heinz NA, Snyder GJ. High thermoelectric figure of merit in PbTe alloys demonstrated in PbTe–CdTe. *Adv Energy Mater*. 2012;2(6):670-675.
30. Cohen I, Kaller M, Komisarchik G, Fuks D, Gelbstein Y. Enhancement of the thermoelectric properties of n-type PbTe by Na and Cl co-doping. *J Mater Chem C*. 2015;3(37):9559-9564.
31. Guttmann GM, Dadon D, Gelbstein Y. Electronic tuning of the transport properties of off-stoichiometric PbxSn1−xTe thermoelectric alloys by Bi2Te3 doping. *J Appl Phys*. 2015;118(6):065102.
32. Zhu T, Fu C, Xie H, Liu Y, Zhao X. High efficiency half-Heusler thermoelectric materials for energy harvesting. *Adv Energy Mater*. 2015;5(19):1500588.
33. Fu C, Zhu T, Pei Y, et al. High band degeneracy contributes to high thermoelectric performance in p-type half-Heusler compounds. *Adv Energy Mater*. 2014;4:1400600.
34. He R, Zhu H, Sun J, et al. Improved thermoelectric performance of n-type half-Heusler MCo1-xNixSb (M = Hf, Zr). *Mater Today Phys*. 2017;1:24-30.
35. Appel O, Gelbstein Y. A comparison between the effects of Sb and 0i doping on the thermoelectric properties of the

$Ti_{0.3}Zr_{0.35}Hf_{0.35}NiSn$ half-Heusler alloy. *J Electron Mater*. 2013; 43(6):1976-1982.
36. Li W, Zheng L, Ge B, et al. Promoting SnTe as an eco-friendly solution for p-PbTe thermoelectric via band convergence and interstitial defects. *Adv Mater*. 2017;29(17):1605887.
37. Li W, Chen Z, Lin S, et al. Band and scattering tuning for high performance thermoelectric Sn1−xMnxTe alloys. *J Materiom*. 2015;1(4):307-315.
38. Banik A, Roychowdhury S, Biswas K. The journey of tin chalcogenides towards high-performance thermoelectrics and topological materials. *Chem Commun (Camb)*. 2018;54(50): 6573-6590.
39. Liu W, Tan X, Yin K, et al. Convergence of conduction bands as a means of enhancing thermoelectric performance of n-type Mg_2Si_1-xSnx solid solutions. *Phys Rev Lett*. 2012;108(16): 166601.
40. Liu X, Zhu T, Wang H, et al. Low electron scattering potentials in high performance Mg2Si0.45Sn0.55 based thermoelectric solid solutions with band convergence. *Adv Energy Mater*. 2013;3(9): 1238-1244.
41. Sadia Y, Aminov Z, Mogilyansky D, Gelbstein Y. Texture anisotropy of higher manganese silicide following arc-melting and hot-pressing. *Intermetallics*. 2016;68:71-77.
42. Hazan E, Ben-Yehuda O, Madar N, Gelbstein Y. Functional graded germanium-Lead Chalcogenide-based thermoelectric module for renewable energy applications. *Adv Energy Mater*. 2015;5(11): 1500272.
43. Hong M, Chen ZG, Yang L, et al. Realizing zT of 2.3 in Ge1-x-y Sbx Iny Te via reducing the phase-transition temperature and introducing resonant energy doping. *Adv Mater*. 2018;30(11): 1705942.
44. Li J, Zhang X, Chen Z, et al. Low-symmetry rhombohedral GeTe thermoelectrics. *Joule*. 2018;2(5):976-987.
45. Hazan E, Madar N, Parag M, Casian V, Ben-Yehuda O, Gelbstein Y. Effective electronic mechanisms for optimizing the thermoelectric properties of GeTe-rich alloys. *Adv Electron Mater*. 2015;1(11):1500228.
46. Zhang J, Song L, Pedersen SH, Yin H, Hung LT, Iversen BB. Discovery of high-performance low-cost n-type Mg3Sb2-based thermoelectric materials with multi-valley conduction bands. *Nat Commun*. 2017;8:13901.
47. Wang X, Li J, Wang C, et al. Orbital alignment for high performance thermoelectric YbCd2Sb2 alloys. *Chem Mater*. 2018;30(15): 5339-5345.
48. Lin SQ, Li W, Chen ZW, Shen JW, Ge BH, Pei YZ. Tellurium as a high-performance elemental thermoelectric. *Nat Commun*. 2016; 7:10287.
49. Veis AN, Ukhanov YI. Study of the absorption coefficient of p-type PbTe. *Soviet Phys Semiconduct*. 1976;10(7):780-783.
50. Rogers L. Light hole mobility in PbTe:Na. *J Phys D Appl Phys*. 1968;1(8):1067-1070.
51. Herman F, Kortum RL, Ortenburger IB, Van Dyke JP. Relativistic band Struture of GeTe, SnTe, PbTe, PbSe and PbS. *J Phys Colloques*. 1968;29:62-77.
52. Pei YZ, Zheng LL, Li W, et al. Interstitial point defect scattering contributing to high thermoelectric performance in SnTe. *Adv Electron Mater*. 2016;2(6):1600019.
53. Zhou M, Gibbs ZM, Wang H, et al. Optimization of thermoelectric efficiency in SnTe: the case for the light band. *Phys Chem Chem Phys*. 2014;16(38):20741-20748.
54. Tang J, Gao B, Lin SQ, et al. Manipulation of band structure and interstitial defects for improving thermoelectric SnTe. *Adv Funct Mater*. 2018;28(34):1803586.
55. Li JQ, Huang S, Chen ZP, et al. Phases and thermoelectric properties of SnTe with (Ge, Mn) co-doping. *Phys Chem Chem Phys*. 2017;19(42):28749-28755.
56. Zheng LL, Li W, Lin SQ, Li J, Chen ZW, Pei YZ. Interstitial defects improving thermoelectric SnTe in addition to band convergence. *ACS Energy Lett*. 2017;2(3):563-568.
57. Banik A, Shenoy US, Anand S, Waghmare UV, Biswas K. Mg alloying in SnTe facilitates valence band convergence and optimizes thermoelectric properties. *Chem Mater*. 2015;27(2): 581-587.
58. Zhang LJ, Qin P, Han C, et al. Enhanced thermoelectric performance through synergy of resonance levels and valence band convergence via Q/In (Q = Mg, Ag, Bi) co-doping. *J Mater Chem A*. 2018;6(6):2507-2516.
59. He J, Xu J, Liu G-Q, et al. Enhanced thermopower in rock-salt SnTe–CdTe from band convergence. *RSC Adv*. 2016;6(38):32189-32192.
60. Tan XJ, Shao HZ, He J, et al. Band engineering and improved thermoelectric performance in M-doped SnTe (M = Mg, Mn, Cd, and Hg). *Phys Chem Chem Phys*. 2016;18(10):7141-7147.
61. Tan G, Zhao LD, Shi F, et al. High thermoelectric performance of p-type SnTe via a synergistic band engineering and nanostructuring approach. *J Am Chem Soc*. 2014;136(19):7006-7017.
62. Al Rahal Al Orabi R, Mecholsky NA, Hwang J, et al. Band degeneracy, low thermal conductivity, and high thermoelectric figure of merit in SnTe–CaTe alloys. *Chem Mater*. 2015;28(1):376-384.
63. Tan GJ, Shi FY, Doak JW, et al. Extraordinary role of Hg in enhancing the thermoelectric performance of p-type SnTe. *Energ Environ Sci*. 2015;8(1):267-277.
64. Tang J, Yao Z, Chen Z, et al. Maximization of transporting bands for high-performance SnTe alloy Thermoelectrics. *Mater Today Phys*. 2019;9:100091.
65. Tang J, Gao B, Lin S, et al. Manipulation of solubility and interstitial defects for improving thermoelectric SnTe alloys. *ACS Energy Lett*. 2018;3(8):1969-1974.
66. Gurieva EA, Prokofeva LV, Stilbans LS, Tamarchenko VI. Thermoelectric figure of merit of Pbte-Snte alloys. *Soviet Phys Semiconduct*. 1975;9(6):809-810.
67. Efimova BA, Kolomoets LA. Thermoelectric properties of Pbte-Snte solid solutions. *Soviet Phys Solid State*. 1965;7(2):339-344.
68. Li J, Chen Z, Zhang X, et al. Simultaneous optimization of carrier concentration and alloy scattering for ultrahigh performance GeTe Thermoelectrics. *Adv Sci (Weinh)*. 2017;4(12):1700341.
69. Lewis JE. Band structure and nature of lattice defects in GeTe from analysis of electrical properties. *Phys Stat Sol*. 1969;35: 737-745.
70. Santhanam S, Chaudhuri AK. Transport properties of SnTe interpreted by means of a two valence band model. *Mater Res Bull*. 1981;16:911-917.
71. Brady EL. Preparation and properties of PbTe. *J Electrochem Soc*. 1954;101(9):466-473.

72. Brebrick RF. Deviations from stoichiometry and electrcial properties in SnTe. *J Phys Chem Solid*. 1963;24:27-36.
73. Rogacheva E. Nonstoichiometry and Properties of SnTe Semiconductor Phase of Variable Composition. *Stoichiometry and Materials Science - When Numbers Matter*; Norderste: Books on demand 2012.
74. Brebrick RF, Gubner E. Composition stability limits of Pbte. 2. *J Chem Phys*. 1962;36(5):1283-1289.
75. Miotkowska S, Kachniarz J, Dynowska E, Story T, Jedrzejczak A. Solubility limit of Mn in the semimagnetice semiconductor. *J Cryst Growth*. 1997;172:455-458.
76. LaLonde AD, Ikeda T, Snyder GJ. Rapid consolidation of powdered materials by induction hot pressing. *Rev Sci Instrum*. 2011; 82(2):025104.
77. Zhou Z, Uher C. Apparatus for Seebeck coefficient and electrical resistivity measurements of bulk thermoelectric materials at high temperature. *Rev Sci Instrum*. 2005;76:023901.
78. Pei Y, LaLonde AD, Wang H, Snyder GJ. Low effective mass leading to high thermoelectric performance. *Energ Environ Sci*. 2012;5(7):7963-7969.
79. Pei YZ, May AF, Snyder GJ. Self-tuning the carrier concentration of PbTe/Ag_2Te composites with excess Ag for high thermoelectric performance. *Adv Energy Mater*. 2011;1(2):291-296.
80. Blachnik R, Igel R. Thermodynamic properties of IV-VI compounds Lead Chalcogenides. *Z Naturforsch B*. 1974;29(9–10): 625-629.
81. Lyden HA. Measurement of the conductivity effective mass in semiconductors using infrared reflection. *Phys Rev*. 1964;134(4A): A1106-A1112.
82. Lewis JE. Optical properties and energy gap of GeTe from reflectance studies. *Phys Status Solidi*. 1973;59:367.
83. Riedl HR, Dixon JR, Schoolar RB. The electric-susceptibility hole mass and optical dielectric constant of SnTe. *Solid State Commun*. 1965;3:323-325.
84. Dziawa P, Kowalski BJ, Dybko K, et al. Topological crystalline insulator states in $Pb_{1-x}Sn_xSe$. *Nat Mater*. 2012;11:1023-1027.
85. Roychowdhury S, Shenoy US, Waghmare UV, Biswas K. Tailoring of electronic structure and thermoelectric properties of a topological crystalline insulator by chemical doping. *Angew Chem Int Ed Engl*. 2015;54(50):15241-15245.
86. Li W, Wu Y, Lin S, et al. Advances in environment-friendly SnTe thermoelectrics. *ACS Energy Lett*. 2017;2(10):2349-2355.
87. May AF, Toberer ES, Saramat A, Snyder GJ. Characterization and analysis of thermoelectric transport in n-type $Ba_8Ga_{16-x}Ge_{30+x}$. *Phys Rev B*. 2009;80(12):125205.
88. Cahill DG, Watson SK, Pohl RO. Lower limit to the thermal conductivity of disordered crystals. *Phys Rev B*. 1992;46(10):6131-6140.
89. Chen Z, Zhang X, Lin S, Chen L, Pei Y. Rationalizing phonon dispersion for lattice thermal conductivity of solids. *Natl Sci Rev*. 2018;0:1-7.
90. Snyder GJ, Agne MT, Gurunathan R. Thermal conductivity of complex materials. *Natl Sci Rev*. 2019;6:380-381.
91. Anderson OL. A simpified method for calculating the Debye temperature from eleastic constants. *J Phys Chem Solid*. 1963;24: 909-917.
92. Sanditov DS, Belomestnykh VN. Relation between the parameters of the elasticity theory and averaged bulk modulus of solids. *Tech Phys+*. 2011;56(11):1619-1623.

SUPPORTING INFORMATION

Additional supporting information may be found online in the Supporting Information section at the end of this article.

How to cite this article: Yao Z, Li W, Tang J, et al. Solute manipulation enabled band and defect engineering for thermoelectric enhancements of SnTe. *InfoMat*. 2019;1:571–581. https://doi.org/10.1002/inf2.12044